JOURNAL OF PETROLOGY | VOLUME 45 | NUMBER 7 | PAGES 1297–1310 | 2004 | DOI: 10.1093/petrology/egh007

Formation of Carbon and Hydrogen Species in Magmas at Low Oxygen Fugacity

A. KADIK[1], F. PINEAU[2]*, Y. LITVIN[3], N. JENDRZEJEWSKI[2], I. MARTINEZ[2] AND M. JAVOY[2]

[1]V. I. VERNADSKY INSTITUTE OF GEOCHEMISTRY AND ANALYTICAL CHEMISTRY, RUSSIAN ACADEMY OF SCIENCES, KOSYGIN ST. 19, MOSCOW, 117975, RUSSIA

[2]LABORATOIRE DE GÉOCHIMIE DES ISOTOPES STABLES, UNIVERSITÉ DE PARIS 7 ET IPGP, 2 PLACE JUSSIEU, 75251 PARIS CEDEX 05, FRANCE

[3]INSTITUTE OF EXPERIMENTAL MINERALOGY, RUSSIAN ACADEMY OF SCIENCES, CHERNOGOLOVKA, MOSCOW DIST., 142432, RUSSIA

RECEIVED MAY 30, 2002; ACCEPTED NOVEMBER 18, 2003

Studies of iron-bearing silicate melt (ferrobasalt) + iron metallic phase + graphite + hydrogen equilibria show that carbon and hydrogen solubilities in melts are important for the evolution of the upper mantle. In a series of experiments conducted at 3·7 GPa and 1520–1600°C, we have characterized the nature (oxidized vs reduced) and quantified the abundances of C- and H-compounds dissolved in iron-bearing silicate melts. Experiments were carried out in an anvil-with-hole apparatus permitting the achievement of equal chemical potentials of H_2 in the inner Pt capsule and outer furnace assembly. The fO_2 for silicate melt–iron equilibrium was 2·32 ± 0·04 log units below iron–wüstite (IW). The ferrobasalt used as starting material experienced a reduction of its iron oxides and silicate network. The counterpart was a liberation of oxygen reacting with the hydrogen entering the capsule. The amount of H_2O dissolved in the glasses was measured by ion microprobe and by step-heating and was found to be between 1 and 2 wt %. The dissolved carbon content was found to be 1600 ppm C by step-heating. The speciation of C and H components was determined by IR and Raman spectroscopy. It was established that the main part of the liberated oxygen was used to form OH^- and to a much lesser extent H_2O, and only traces of H_2, CO_2 and CO_3^{2-}. Dissolved carbon is mainly present as atomic carbon or amorphous carbon. It was possible to measure an isotopic fractionation of 0·8‰ between graphite and dissolved or amorphous carbon at the temperatures of experiments. The Raman spectra also suggest that the network units might contain Si–C bonds. Comparison of our results with the literature demonstrates that the amount of dissolved species decreases as fO_2 decreases. In the light of these experimental data, it appears that large-scale melting of the proto-Earth could be associated with melts containing an oxidized form of hydrogen. The early Earth, however, was likely to have been a very reducing environment, in which most of the carbon remained stable in the form of graphite. As the Earth became more and more oxidized, melts formed at depth would have dissolved larger amounts of water, and also carbon in the form of CO_2, which would have made the degassing of the upper mantle more and more efficient.

KEY WORDS: *ferrobasalts; experimental petrology; oxygen fugacity; stable isotopes*

INTRODUCTION

It is generally accepted that most of the present-day upper mantle is moderately oxidized at oxygen fugacities well above metal saturation. The application of olivine–orthopyroxene–spinel phase equilibrium methods to measure the oxygen fugacity (fO_2) at which upper-mantle peridotites equilibrated has led to the consensus that the lithospheric upper mantle is, nearly everywhere, relatively oxidized, the majority of samples falling within −3 to +1 log units (bars) of the fayalite–magnetite–quartz oxygen buffer (ΔFMQ = −3 to +1) (Wood *et al.*, 1990; Ballhaus, 1993). Fluids identified in mantle samples are also oxidized, and consist mainly of $CO_2 + H_2O$. So far, the most reduced samples from cratonic Archean lithosphere plot as low as ΔFMQ = −3 to −5 (Mattioli

*Corresponding author. Telephone: 33 1 44 27 28 11. Fax: 33 1 44 27 28 30. E-mail: pineau@ipgp.jussieu.fr

et al., 1989; Wood *et al.*, 1990; Daniels & Gurney, 1991; Ballhaus, 1993; Kadik, 1997; Parkinson & Arculus, 1999). These low fO_2 values are considered to provide evidence that the upper mantle was originally more reduced and has become progressively more oxidized with time (e.g. Arculus, 1985), and that at least part of the upper mantle is reduced enough to stabilize carbon and CH_4 at depth. One consequence of this observation is that even the parts of the upper mantle at the lower end of the recorded range have fO_2 values 2–3 log units more oxidized than that appropriate for chemical equilibrium with an Fe-rich metallic phase (O'Neill & Wall, 1987). If the average mantle olivine (Fo_{91}) was in chemical equilibrium with core-forming iron, the fO_2 would be at least 5 log units more reduced than the present-day upper-mantle value.

It has been argued that the composition and oxidation state of the mantle is the result of heterogeneous accretion with more than one core-forming event as proposed by Arculus *et al.* (1990), with the addition of an oxidized 'late veneer' (Wanke, 1981; Javoy, 1997), or of an auto-redox process in the upper mantle (O'Neill, 1991; Javoy, 1995; Galimov, 1998). O'Neill & Pownceby (1993), Ballhaus (1995) and Wood (1995) have proposed that the present-day mantle becomes more reduced with increasing depth. Crystal-chemistry considerations (molar volume effect, changes in solid solution, phase transitions and the incorporation of Fe^{3+} in the spinelloid phases) require that fO_2 declines with respect to the FMQ buffer as depth increases. This suggests that the convecting upper mantle may become saturated with an Fe-dominated metal phase at a depth of around 300 km.

Although the oxidized nature of the upper mantle is still subject to debate, it is plausible that the relative abundances of H and C species under reduced conditions play an important role in partial melting of the present-day mantle as a whole. However, the nature of mantle partial melting under reduced conditions in the presence of graphite and C–O–H volatiles is still not clear. The following studies have investigated different synthetic systems in the presence of reduced volatiles: Eggler & Baker (1982) examined the effect of C–H volatiles on melting of the diopside $(Di)_{35}$–pyrope $(Py)_{65}$ system at 20 GPa and fO_2 near the Si–SiO_2 buffer; Taylor & Green (1987) explored the system nepheline–forsterite–silica–methane-dominated fluid at 2·8 GPa, 1300°C and fO_2 at IW − 5 (where IW is the iron–wüstite buffer); Holloway & Jakobsson (1986) measured the solubility of CO_2, CO, CH_4, H_2, and H_2O in silicate melts at 1–2 GPa, 1200°C where the C–O–H phase was buffered by graphite, iron and wüstite; Luth *et al.* (1987) studied the H_2 solubility in melts of $NaAlSi_3O_8$ composition; and Holloway *et al.* (1992) and Kadik (1996) considered the dissolution of free carbon (graphite) in basaltic melt at variable pressure and fO_2. Holloway & Jakobsson (1986) and Taylor & Green (1987) have shown that low fO_2 produces a general reduction of the silicate network, with C–H species dissolved as H_2O, OH^-, and CO_3^{2-}. Dissolution of free carbon may be the source of CO_3^{2-} (Holloway *et al.*, 1992) or C^{2-} in melt (Swisher, 1968). It is expected that interaction of carbon and its volatile compounds with a silicate melt strongly depends on fO_2, correspondingly changing the forms of its stability in silicate liquids to CO_2, CO_2^{3-}, Si–C, and C–Me (Ca, Mg, Fe). Nevertheless, these specific features of carbon dissolution in many ways remain unclear.

In this paper, our major concern is to look at the speciation and concentration of carbon and hydrogen when they dissolve in a melt, and the possible implications for upper-mantle evolution. We will show the role that melting of a reduced carbon-bearing upper-mantle source plays in the generation of oxidized C–O–H volatiles. The model for the Earth's formation proposed by Javoy (1995, 1997, 1999) is based, among other features, on the equivalence of the oxygen isotopic composition of enstatite chondrites (EH) with that of the Earth and Moon. More than 99% of the Earth could be formed from such meteoritic parental material, and the balance by a late veneer of carbonaceous chondrite (CI) or comet-like material. The proto-Earth (formed from pure EH) could host about 50% of the final carbon content of the present Earth and only 6% of the hydrogen, and would have been very reduced (fO_2 IW − 3 to IW − 5). It would have contained very little or no oxidized iron, only reduced forms of carbon and almost no water. Core formation induced by the major impact during the creation of the Moon initiated nearly complete melting of the mantle. The upper mantle left after the main core-forming iron extraction event would still have been reduced and contained more iron than the present upper mantle, and a carbonaceous phase such as graphite, diamond or carbide. The Earth would still have been hot, and Fe-rich magmas probably existed. The late veneer brought 94% of the hydrogen and about 50% of the carbon (in the form of hydrous minerals, complex hydrocarbon molecules and carbonates). The recycling of the late veneer is the source of the oxygen needed to reach the level of oxidation of the proto-mantle. Our study of the system graphite–ferrobasalt at low fO_2 (IW − 2 to IW − 3), 3·7 GPa and 1520–1600°C is an attempt to model experimentally, with more details than previous work, the equilibrium between oxidized and reduced forms of C- and H-components present in a melt formed under reduced conditions.

HIGH-PRESSURE EXPERIMENTS

Experimental techniques

Experiments were carried out in an anvil-with-hole apparatus at 3·7 GPa, 1520–1600°C and controlled

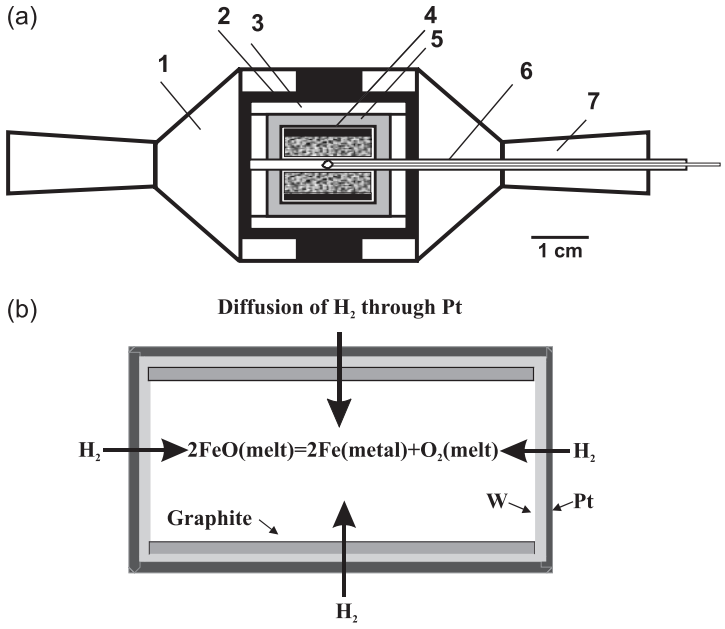

Fig. 1. The experiment at reducing conditions. (**a**) Schematic representation of the anvil-with-hole apparatus: 1, container (lithographic limestone); 2, heater (high-purity graphite); 3, sample holder (MgO: BN_{hex} = 3:1, weight ratio); 4, sealed Pt capsule lined with W foil; 5, buffer mixture (pressed Fe_2O_3); 6, thermocouple, Pt + 30%Rh/Pt + 6%Re; 7, ceramic sleeve. (**b**) Schematic regime of H_2. An experiment under reducing conditions includes the following stages: 1, H_2 diffusion into the platinum capsule from the buffer assemblage; 2, formation of Fe alloy and liberation of O_2; 3, interaction of H and O with melts and graphite, formation of an 'oxidized bond' and 'reduced bond'.

hydrogen (oxygen) activity as described by Litvin (1989). The device is a 2000 tons uniaxial press, equipped with a high-pressure system consisting of a pair of tungsten carbide anvils with holes and a cell (Fig. 1a). Each hole is a truncated cone. Two anvils are axially and oppositely directed, separated by pyrophyllite gaskets. They form a cavity that holds the sample assembly. The space inside the heater is 6 cm^3, and characterized by a uniform distribution of temperature (±5°C) and pressure (±0·1 GPa). The sample is placed in a sealed Pt capsule 10 mm in diameter and 5 mm in height. Two capsules of this type are used in one assembly. The temperature is measured by a Pt30%Rh/Pt6%Rh thermocouple in a radial position, with its junction in the centre of the cell assembly (between the capsules). The accuracy of temperature measurements is ±5°C at 1500°C and close to ±10°C at 1600°C. Pressure is determined at room temperature with Bi-based transducers incorporated in each cell assembly. Pressures at high temperatures were calibrated using the quartz–coesite transition (Bohlen & Boettcher, 1982). The reproducibility of experimental pressures in the cell assembly is estimated as ±0·1 GPa.

Silicate composition in the ferrobasalt–graphite system was prepared from a natural basaltic rock (in wt %: Na_2O 2·68, MgO 4·98, Al_2O_3 13·12, SiO_2 49·18, K_2O 0·36, CaO 8·40, TiO_2 1·95, MnO 0·28, FeO 18·01, P_2O_5 0·22). Starting materials were powdered glasses. Samples were melted in the presence of N_2 at 1250°C in alundum crucibles, and quenched in air to colourless glasses; their composition and homogeneity were checked by microprobe analysis. The charges consisted of 200–300 mg of powdered glass topped by a graphite disc 0·2 mm thick (Fig. 1a). They were isolated from the Pt capsule walls by tungsten foil (0·05 mm thick), which reduces the interaction between the Fe-bearing melt and platinum (Litvin, 1989). The run duration varied between 30 and 120 min at 1500–1600°C. The experiments were quenched by turning off the power. The initial quench rate was ~200°C/s.

Regime of hydrogen and oxygen fugacity

The technique of fO_2 buffering employed here relies upon the diffusion of H_2 through Pt to achieve equal chemical potentials of H_2 in the inner Pt capsule and outer solid fO_2 buffer assembly in the presence of H_2O. Ulmer & Luth (1991) used a similar method to investigate graphite–C–O–H fluid equilibria. In the case of our experiments the fH_2 was buffered by the furnace assembly functions at the iron (Fe)–wüstite (FeO) buffer. Under such conditions, the fH_2O/fH_2 ratio in the O–H system is fixed at a given pressure and temperature. The fO_2 imposed on the charge by graphite is controlled by the equilibrium between graphite, H_2 buffered externally, and the reduction of the Fe-bearing melt with liberation of O_2 (Fig. 1b). If a C–O–H fluid is present, the fO_2 (Fig. 2) and the C–O–H fluid composition (Fig. 3) would correspond to the equilibrium values in a C–O–H system at a given P and T. A feature of our experiments

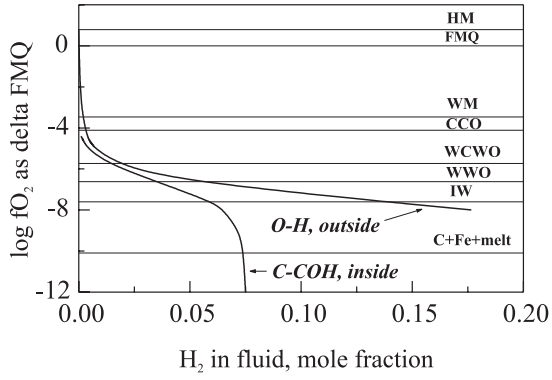

Fig. 2. The relative oxygen fugacity (with respect to FMQ buffer) of a separate C–O–H fluid in equilibrium with elemental carbon plotted against the H_2 mole fraction in the fluid at 40 kbar and 1500°C. Also shown is the position of solid-state buffers: fayalite–magnetite–quartz (FMQ), magnetite–haematite (MH), wüstite–magnetite (WM) and iron–wüstite (IW) (Chou, 1987). The upper elemental carbon stability limit is given by the equilibrium $C + O_2 = CO_2$ (CCO). The upper stability limit of the tungsten foil and WC is given by the equilibria $W + O_2 = WO_2$ (WWO) and $WC + O_2 = WO_2 + C$ (WCWO) (O'Neill & Pownceby, 1993; Taylor & Foley, 1989). Calculated values (see text) of the fO_2 values for ferrobasaltic melt + graphite + iron equilibrium (C + Fe + melt) during experiments at 3·7 GPa and 1520–1600°C are shown.

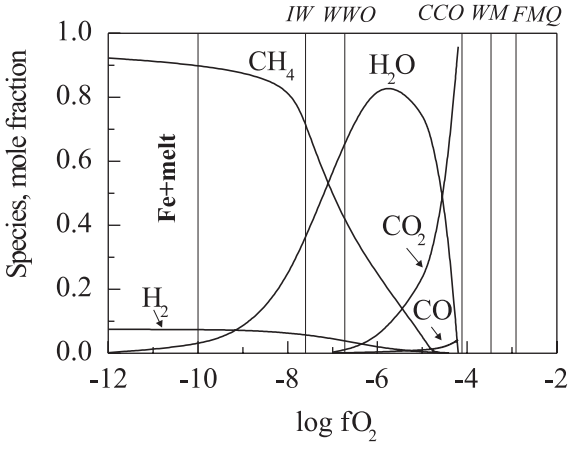

Fig. 3. The fO_2 values of a C–O–H fluid in equilibrium with graphite with fH_2 imposed by H–O equilibrium outside a Pt capsule at 4 GPa and 1500°C. The C–O–H equilibrium has been calculated using the modified Redlich–Kwong formulation (MRK) (Holloway, 1981). Oxygen buffers are shown for reference and are labelled as in Fig. 2.

is that they were carried out under C–O–H fluid-absent conditions (inside the capsules), verified by the absence of bubbles at any observable scale. In theory, the fO_2, which corresponds to the phase equilibrium during the experiments, is dominated by the reaction

$$\mathrm{FeO\ (melt)} = \mathrm{Fe\ (alloy)} + \tfrac{1}{2}\mathrm{O_2} \qquad (1)$$

corresponding to the reduction of an iron-bearing melt under the influence of H_2 diffusion through Pt. Calculations demonstrate that, at a given fH_2 in the system, the fO_2 of a C–O–H-bearing melt inside the Pt capsule should be much lower than the fO_2 of an O–H fluid phase outside the Pt capsule (see Fig. 2 and figure caption for details).

Oxidation state of the C–O–H-bearing glasses after the experiment

Metal–silicate partition coefficients depend strongly on fO_2 (see, e.g. Hillgren *et al.*, 1994). Normally the fO_2 of such experiments is calculated based on a calibration of the IW buffer along with the concentrations of FeO in the silicate and of Fe in the metal [see equation (1)].

The equilibrium constant for reaction (1) is

$$\log K = \log\left(a_{\mathrm{FeO}}/a_{\mathrm{Fe}}\right) - \tfrac{1}{2}\log fO_2^{\mathrm{exp}} \qquad (2)$$

where $\log fO_2^{\mathrm{exp}}$ is the fO_2 of the high-pressure experiment. The equilibrium constant for the reaction between pure Fe and pure FeO (which defines the IW buffer), with $a_{\mathrm{Fe}} = 1$ and $a_{\mathrm{FeO}} = 1$, reduces to

$$\log K = -\tfrac{1}{2}\log fO_2^{\mathrm{IW}} \qquad (3)$$

where $\log fO_2^{\mathrm{IW}}$ gives the oxygen fugacity of the Fe–FeO equilibrium under the P–T conditions of the experiment.

The fO_2 of the experiment may also be expressed relative to the IW buffer curve:

$$\log fO_2^{\mathrm{exp}} = \log fO_2^{\mathrm{IW}} - \Delta\mathrm{IW} \qquad (4)$$

where ΔIW is the difference between $\log fO_2^{\mathrm{IW}}$ and the fO_2 of the experiment ($\log fO_2^{\mathrm{exp}}$). Combining equations (2), (3) and (4) gives

$$\log\left(a_{\mathrm{FeO}}/a_{\mathrm{Fe}}\right) - \tfrac{1}{2}(\log fO_2^{\mathrm{IW}} - \Delta\mathrm{IW}) = -\tfrac{1}{2}\log fO_2^{\mathrm{IW}} \qquad (5)$$

and thus

$$2\log\left(a_{\mathrm{FeO}}/a_{\mathrm{Fe}}\right) = \Delta\mathrm{IW} \qquad (6)$$

where a_{FeO} and a_{Fe} are the activities of FeO and Fe in iron-bearing melt and metal, respectively. Inserting the respective activities of Fe and FeO in the product phases into equation (6) thus allows the fO_2 to be determined relative to the Fe–FeO equilibrium. The activity coefficient for FeO in the melt at 1520–1600°C was calculated from Ariskin *et al.* (1993). The fO_2 for the melt–iron equilibrium yields an fO_2 of 2·26–2·37 log units below IW ($\Delta\log fO_2^{\mathrm{IW}} = -2{\cdot}37$ for Fb148-gl, $\Delta\log fO_2^{\mathrm{IW}} = -2{\cdot}33$ for Fb150-gl and $\Delta\log fO_2^{\mathrm{IW}} = -2{\cdot}26$ for Fb231-gl).

RESULTS

Three runs were completed at 3·7 GPa in a narrow range of temperature (1520–1600°C) and $\Delta\log fO_2^{\mathrm{IW}} = -2{\cdot}32 \pm 0{\cdot}06$. The experimental conditions of each run are given

Table 1: Electron microprobe analyses of run products: clear glass, glass with quench dispersed graphite (C) and Fe alloy after experiments at 3·7 GPa, 1520–1600°C

Sample	Quench product		Na_2O	MgO	Al_2O_3	SiO_2	K_2O	CaO	TiO_2	MnO	FeO	P_2O_5	Total
Glass													
Fb148-gl	Clear glass	Average (5)	2·83	5·31	13·36	52·34	0·34	9·17	2·24	0·26	10·22	0·11	96·55
		SD	0·05	0·09	0·47	1·07	0·02	0·19	0·07	0·03	0·18	0·02	1·64
Fb148-bl	Glass + quench C	Average (3)	2·89	5·09	14·44	53·22	0·39	8·96	2·05	0·25	10·41	0·14	97·90
		SD	0·00	0·19	0·24	0·44	0·00	0·12	0·15	0·07	0·06	0·02	1·15
Fb150-gl	Clear glass	Average (8)	2·89	5·34	13·91	53·30	0·38	9·19	2·15	0·24	11·26	0·18	98·99
		SD	0·05	0·08	0·25	0·55	0·01	0·11	0·08	0·02	0·19	0·05	0·49
Fb150-bl	Glass + quench C	Average (3)	2·96	4·84	13·95	52·46	0·30	9·59	2·26	0·28	13·17	n.d.	99·81
		SD	0·17	0·09	0·21	0·95	0·02	0·25	0·07	0·06	1·03		0·52
Fb231-gl	Clear glass	Average (5)	2·80	5·04	13·74	52·21	0·37	8·89	2·07	0·29	11·73	0·18	97·44
		SD	0·08	0·14	0·09	0·49	0·01	0·06	0·04	0·02	0·28	0·03	0·83
Fb231-bl	Glass + quench C	Average (5)	2·78	4·90	13·97	53·29	0·28	9·42	2·16	0·3	12·04	0·18	99·32
		SD	0·08	0·17	0·10	0·65	0·03	0·25	0·07	0·08	0·51	0·03	0·08

Sample	Quench product		Fe	Co	Ni	Si	P	W	Pt	Total
Fe alloy										
Fb148-gl	Spherical droplet	Average (5)	91·30	0·16	0·08	0·17	0·99	4·93	0·99	97·62
		SD	1·27	0·02	0·03	0·07	0·38	0·79	0·38	0·72
Fb150-gl	Spherical droplet	Average (5)	87·85	0·17	0·08	0·27	0·71	2·35	0·04	91·47
		SD	0·99	0·02	0·04	0·11	0·22	0·96	0·04	0·50
Fb231-gl	Spherical droplet	Average (3)	89·74	0·19	0·10	0·08	1·25	0·10	0·13	92·45
		SD	1·48	0·01	0·05	0·02	0·14	0·09	0·18	0·89

in Table 1. The recovered charges were examined microscopically under reflected light using immersion oil. The charges consist of pink glasses containing spherical droplets of metallic iron concentrated at the bottom of the charge (30–100 μm in size) and thin hexagonal and triangular tablets of graphite crystals (100–300 μm in size) visible in transmitted light (Fig. 4a). No bubbles were visible. The charges were studied by a series of techniques to tentatively characterize the form in which carbon and hydrogen were present and their speciation. These techniques included: (1) electron microprobe to visualize the texture and to acquire compositional data for the various phases present; (2) IR spectroscopy to characterize H- and C-species detectable by this technique; (3) Raman spectroscopy, which allowed the characterization of poorly crystallized graphite (which could not be detected by the preceding technique) and the possible presence of Si–C, and further checks for the presence of the OH^- bond; (4) ion probe analysis to measure the amount of hydrogen present in the glasses to compare with the step-heating technique (5); (5) step-heating to quantify the amount of water and carbon present in the glass phases and to look at isotopic fractionation between graphite and the dissolved carbon.

Electron microprobe analysis

Electron microprobe analysis of glasses and iron-rich globules was performed at the Microprobe Camparis Centre of the Université de Paris, with an SX50 Cameca microprobe, four wavelength-dispersive spectrometers (WDS) and one energy-dispersive spectrometer (EDS). At the V. I. Vernadsky Institute of Geochemistry and Analytical Chemistry, Russian Academy of Sciences (Moscow), we used a Camebax microbeam and four wavelength-dispersive spectrometers (WDS) and one energy-dispersive spectrometer (EDS). Polished epoxy mounts containing the samples were coated with carbon. The images obtained by electronic microscopy show that the silicate liquid was not quenched to a glass at the top and bottom parts of the charges, but crystallized dendritically and formed spheroids (50–200 μm in size) as inclusions in clear glass (Fig. 4b–d). The metallic Fe-rich globules are spherical with a dendritic microstructure (Fig. 4d and e), which suggests that this phase was liquid during the experiment. Selected analyses of the phases (clear glasses, glass containing dendritic texture) are given in Table 1. Each glass composition represents at least five analyses. For the glass from the quenched zone, the beam

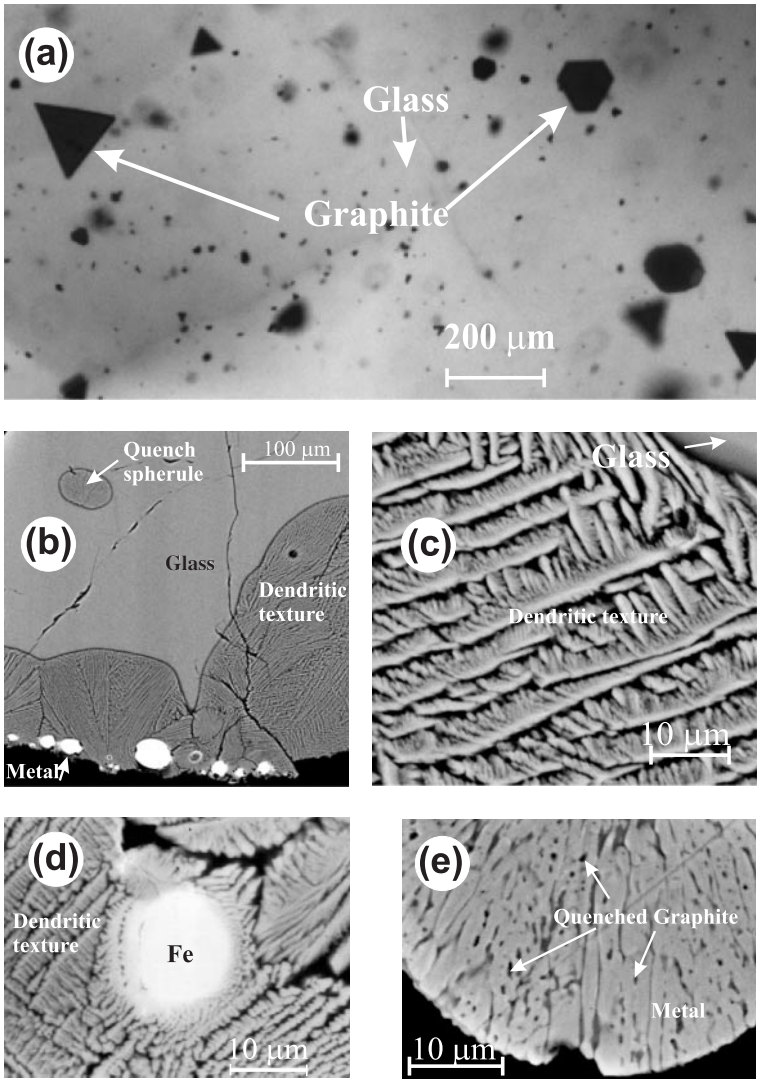

Fig. 4. (a) Optical photomicrograph of the run products in fb148-glass, transmitted light. Thin hexagonal and triangular black tablets are graphite crystals equilibrated with melt. (b)–(e) Backscattered electron photographs of run products (Run 148). (b) Contact between glass (light grey) and the bottom parts of samples with a quenched dendritic microstructure. Dark spheroids in the clear glass are inclusions with a quenched dendritic texture. Bright spherical droplets are the iron metallic phases largely segregated in the bottom region of the charges. Dark area is epoxy. (c) Detailed view of the dendritic texture of the glass and the quench dispersed graphite. (d) Quench dendritic microstructure around metallic iron. (e) Quench graphite dendritic texture within metallic Fe droplets.

was defocused to minimize specimen damage. The fact that a similar chemical composition was found for both clear and dendritic textures indicates that such textures are linked to quenching.

The main feature of the chemical compositions is the decrease of FeO concentration from 18 wt % (FeO content of the starting material) to 10·2–11·7 wt % FeO. This phenomenon reflects reduction of some of the FeO in the starting melts to Fe metal (6·48 wt % Fe for Fb148-gl, 5·85 wt % Fe for Fb150-gl and 5·46 wt % Fe for Fb231-gl). Figure 5 shows melt compositions calculated assuming that part of the reduced FeO has been removed. Comparison of these estimates with the glass compositions (normalized to 100%) demonstrates that the crystallization of Fe is responsible for the melt composition changes. P_2O_5, however, shows much lower contents than those calculated. This is explained by the solubility of P in Fe-phases (0·7–1·25 wt %) and their following simultaneous removal. The Fe contents of the tungsten foils and the Pt capsule are below 0·1 wt %. The contents of Pt in W and W in Pt are also very low (below 0·01–0·1 wt %). Measurement of the samples revealed that, for both metals, the total sum of Pt and W averaged around 99·8%. The iron-rich globules were analysed and compared with known iron–carbon alloys, which allowed the carbon

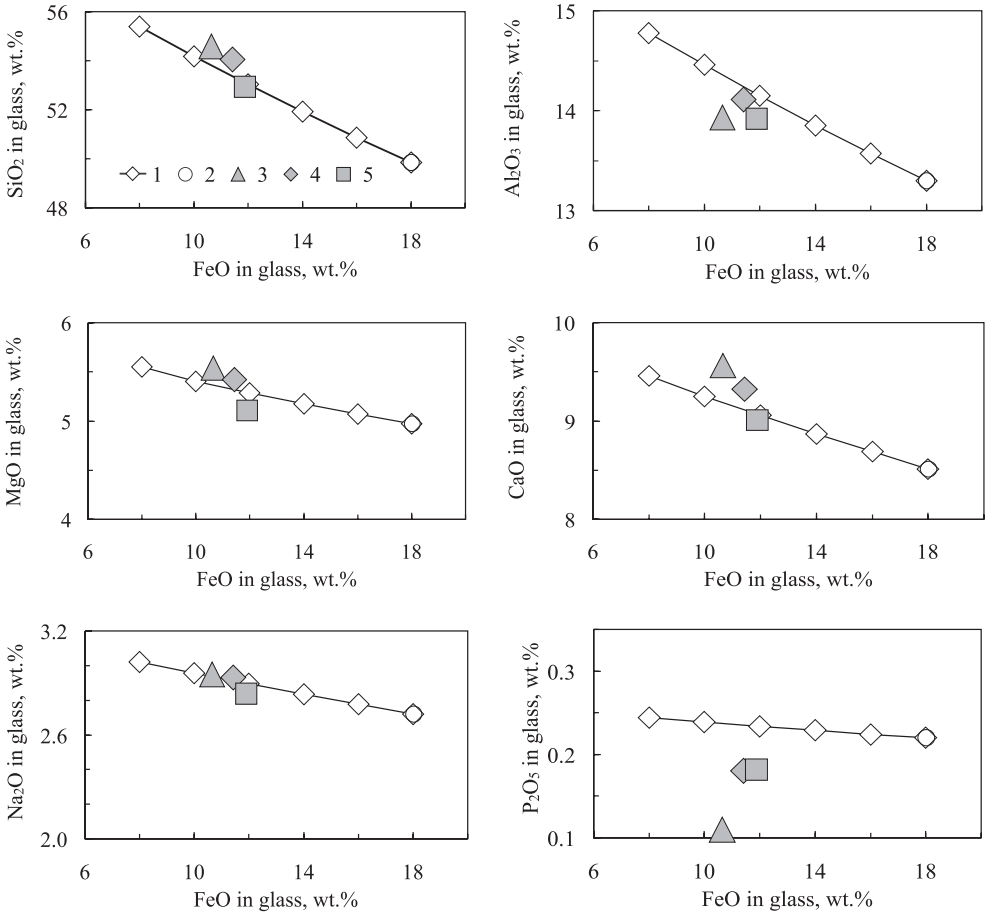

Fig. 5. Compositional variation of C–H-bearing glasses vs wt % FeO as an indicator of the degree of melt reduction. The SiO_2, MgO, CaO and Na_2O contents are close to calculated values. The results for P_2O_5 are significantly different and indicate that the behaviour of this element depends on its solubility in graphite or a metallic Fe phase. Symbols: (1) glass compositions calculated assuming that part of the reduced FeO has been removed; (2) the initial FeO content in the glass; (3), (4), (5) compositions of glasses after experiments Fb-148, Fb-150, Fb-231, respectively.

content of these globules to be fixed between 2·4 and 7·5 wt %.

Infrared spectroscopic study

Doubly polished thick sections were prepared to collect the Fourier transform infrared (FTIR) spectra of the quench products. The thickness of the glasses varied between 80 and 262 μm ± 1 μm. The IR measurements were performed on an FTIR spectrometer (Magna 550, Nicolet) coupled with an optical–IR microscope (LGIS, Paris). Transmission spectra were obtained using the following conditions: MCT_A detector, Ge over KBr beam splitter, 8 cm^{-1} resolution, a mirror velocity of 1·899–3·16 cm/s and a minimum of 300 scans. The aperture diameter was 100 μm. The observed absorption bands in the FTIR spectra were documented for Fb148-gl, Fb150-gl and Fb231-gl samples and they are reported in Table 2. A typical FTIR spectrum of a C–H-bearing glass is illustrated in Fig. 6a.

O–H species. Above 3000 cm^{-1}, a broad, asymmetric band centred at ~3520 cm^{-1} is the most prominent feature in the high-frequency region. This absorption band is due mainly to fundamental OH stretching vibrations of OH groups and H_2O molecules (Stolper, 1982; Newman *et al.*, 1986). The fundamental bending vibration of H_2O molecules corresponds to a sharp peak at 1633–1635 cm^{-1}. The relative proportion of molecular H_2O and hydroxyl group cannot be given, because the molar absorption coefficients are not known for such uncommon melt compositions. The absorption band near 4129–4138 cm^{-1} identified in Fb150-gl (Fig. 6b) may represent the stretching vibration of the H_2 molecule (Dianov *et al.*, 2000).

C–O species. A weak and broad band centred at ~2360–2370 cm^{-1} for Fb148-gl and Fb231-gl (not seen in Fb150-gl) is interpreted as dissolved molecular CO_2. Dissolved carbonates have characteristic absorption band(s) at ~1600–1380 cm^{-1} (Fine & Stolper, 1985). Weak and broad peaks at 1430–1435 cm^{-1}

Table 2: FTIR wavenumber of the different peaks observed and their corresponding absorbance

Sample no.	d^* (μm)	Wavenumber (cm^{-1})					
		1430 ± 3 CO_3^{2-}	1633 ± 3 H_2O	2360–2380 CO_2	3525 ± 10 $OH^- \pm H_2O$	4140 ± 5 H_2	4510 ± 5 OH^-
Absorbances							
Clear glass							
Fb148C-002	180 ± 5	0·01	0·48	0·06	saturated	0·009	n.d.
Fb148C-004	180 ± 5	0·01	0·39	0·05	saturated	0·010	n.d.
Fb148-001†	175 ± 5	0·03	0·98	0·02	saturated	0·005	0·019
Fb148-004†	175 ± 5	0·07	1·49	—	saturated	—	0·020
Fb150-007	80 ± 5	—	0·16	0·02	1·33	—	0·010
Fb150-010	80 ± 5	—	0·20	—	1·84	0·003	0·013
Fb150-011	80 ± 5	—	0·14	0·02	1·39	—	0·013
Fb231-012	262 ± 3	0·07	0·59	0·01	saturated	0·014	0·033
Fb231-017	203 ± 5	0·032	0·43	0·07	saturated	0·009	0·020
Fb231-020	121 ± 2	0·014	0·27	0·05	2·44	0·100	0·010
Fb231-023	241 ± 1	—	0·58	0·09	saturated	0·012	0·030
Glass with quench dispersed graphite							
Fb148C-001	180 ± 5	0·009	0·05	0·05	saturated	0·009	n.d.
Fb148-002	175 ± 5	0·01	0·42	0·05	saturated	0·009	0·020
Fb148-003†	175 ± 5	0·07	1·57	—	saturated	0·010	0·020
Fb231-016	262 ± 3	0·03	0·47	0·07	saturated	0·010	0·028
Fb231-024	241 ± 1	—	0·64	0·07	saturated	0·010	0·030
Fb231-022	121 ± 2	0·02	0·24	0·03	2·30	0·010	0·013

*Thickness of the sample.
†The higher absorbance for 1633 cm^{-1} compared with other measurements reflects structural re-equilibration of the alumosilicate melt network during quenching or local heterogeneity in concentration of hydrogen in glass.

observed in Fb150-gl and Fb231-gl and in part of Fb148-gl samples could represent such species.

Other species. It would be expected that under reduced conditions, C- and H-components other than molecular H_2O, OH^- and CO_2, or carbonate ions could exist in the experimental glasses but cannot be detected by IR spectroscopy. The possible candidates are Si–H, Si–C and C–H. C–H bonds are expected at 3050–2850 cm^{-1}, Si–H bonds at 2250–2100 cm^{-1} and C–H bonds stretching in dissolved molecular methane or other hydrocarbon groups such as $-CH_3$ or $-CH_2-$ at ~2900 cm^{-1} (Pouchert, 1981). However, no such absorption bonds were noted in our charges.

Thus it appears that the main dissolved species correspond to OH^- groups. Most of the H_2O content (e.g. between 1 and 2 wt %) certainly occurs in this form. Molecular water is present but the intensity of the signal is low. Molecular CO_2 and carbonate ions are present only as traces. This means that the carbon content measured by step-heating (see below) is present in a form not detectable by FTIR.

Raman spectroscopic study

Micro-Raman spectroscopy was used to search for dissolved carbon and hydrogen species in quench glasses and graphite or amorphous carbon. The Raman spectroscopy was performed at the Itodys laboratory at Université de Paris 7–IPGP, using a Dilor XY confocal micro-Raman spectrometer, and at the Institute of General Physics of the Russian Academy of Sciences (Moscow). The spectra were corrected for temperature- and frequency-dependent scattering intensity before statistical analysis. A correction factor of the form employed by Long (1977) and given by Neuville & Mysen (1996) was used. The corrected Raman intensities were normalized to the data point of the greatest absolute intensity.

The Raman spectra of the glasses in the high-frequency region (3000–3800 cm^{-1}) show a broad, asymmetric band at ~3560 cm^{-1} (Fig. 7a). The topology of this band is similar to that found for H_2O-bearing glasses by Mysen & Virgo (1986) and for H^--bearing glasses in the system Na_2O–Al_2O_3–SiO_2 by Luth *et al.* (1987). This band is assigned to the stretching vibrations of OH^-

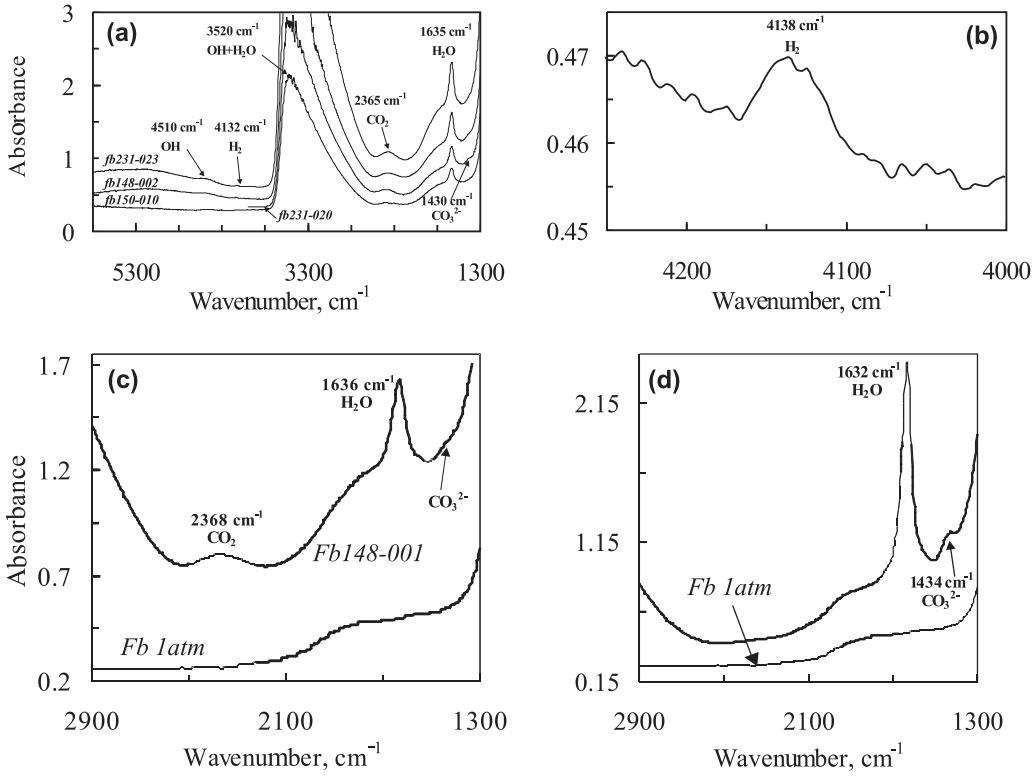

Fig. 6. FTIR spectra of H-bearing quenched glasses. (a) FTIR spectra over the range 6000–1300 cm^{-1} for: the initial ferrobasaltic glass (Fb 1 atm, sample thickness 40 ± 2 μm) quenched from 1 atm at 1300°C and $\Delta \log fO_2 = IW - 2{\cdot}46$ log units; sample Fb148-gl, thickness 175 ± 5 μm; Fb150-gl, $80 \pm 0{\cdot}5$ μm; Fb231-gl, 121 ± 2 μm and 241 ± 1 μm. The wide band near 4500 cm^{-1} is assigned to the OH group. (b) The absorption band near 4138 cm^{-1} (Fb150-gl, $80 \pm 0{\cdot}5$ μm) corresponds to the vibration of the H–H bond. (c) FTIR spectrum in the range 2900–1300 cm^{-1} should show the typical vibration of the C–O bond. The initial ferrobasaltic glass (Fb 1 atm, see Fig. 7a) is compared with sample Fb148-001. A broad, weak band centred at ~2368 cm^{-1} is interpreted as dissolved molecular CO_2. No dissolved carbonate ion was detected. (d) Sample Fb150 shows a weak and broad peak at 1430–1435 cm^{-1} interpreted as dissolved carbonate ion. No dissolved molecular CO_2 was detected.

groups, either in molecular or in OH^- groups bonded to cations in the silicate network.

In the low-frequency region (1200–400 cm^{-1}), our glassy samples show distinct bands at 982 cm^{-1}, 784 cm^{-1} and 514 cm^{-1} (Fig. 7b). These correspond to aluminosilicate band frequencies found in the ranges 500–600 cm^{-1}, 800–850 cm^{-1} and 900–1200 cm^{-1} (as in all aluminosilicates); however, the frequencies and the intensities of the framework vibration bands depend strongly on glass composition (Neuville & Mysen, 1996; Mysen, 1998). For comparison, the initial glass, quenched from 1 atm, 1300°C and $\Delta \log fO_2^{IW} = -2{\cdot}46$ units was the same as during the experiments at 3·7 GPa and 1520–1600°C, and the given activities of C and H. As in the high-pressure experiments, the ferrobasaltic melt was reduced with formation of a metallic Fe phase. This sample exhibits four bands at 1298 cm^{-1}, 1259 cm^{-1}, 912 cm^{-1} and 494 cm^{-1}, similar to the carbon- and hydrogen-bearing glasses, but with decreasing frequencies for the last two. These correspond to aluminosilicate band frequencies (Fig. 7b). In this figure, the sample exposed to 3·7 GPa shows a peak at ~800 cm^{-1}. Spectral features of glasses after high-pressure experiments are considered to represent the influence of hydrogen and carbon on melt structure. For example, Mysen (1998) interpreted the pronounced peak present at 784 cm^{-1} as the Si–OH stretching frequency in the framework for the system K_2O–SiO_2–H_2O. This vibration peak at 784 cm^{-1} can also be assigned to the Si–C band found in moissanite [Debernardi *et al.*, 1999; see also our definitions (Fig. 7c)]. The Raman spectrum we observed for a synthetic moissanite crystal (parallel to the *c*-axis) exhibits two strong bands centred at 784 and 762 cm^{-1}. This is a strong indication that Si–C may be present in our samples. However, this requires further experimental study.

Broad bands are observed at approximately 1347 cm^{-1} and 1604 cm^{-1} (Fig. 7d) in spectra taken with the laser beam focused on the black zones in the region of dendritic microstructure (see Fig. 4c and d). These vibrations correspond to poorly crystallized graphite or amorphous carbon (Lespade *et al.*, 1982). Individual crystals of graphite present in clear glass show sharp bands at 1595 cm^{-1} and no band around 1347 cm^{-1} (Fig. 7e), whereas a graphite disc (located at the top of the sample during the experiment), displays a sharp band at 1585 cm^{-1} and a small one at 1359 cm^{-1}; Fig. 7f).

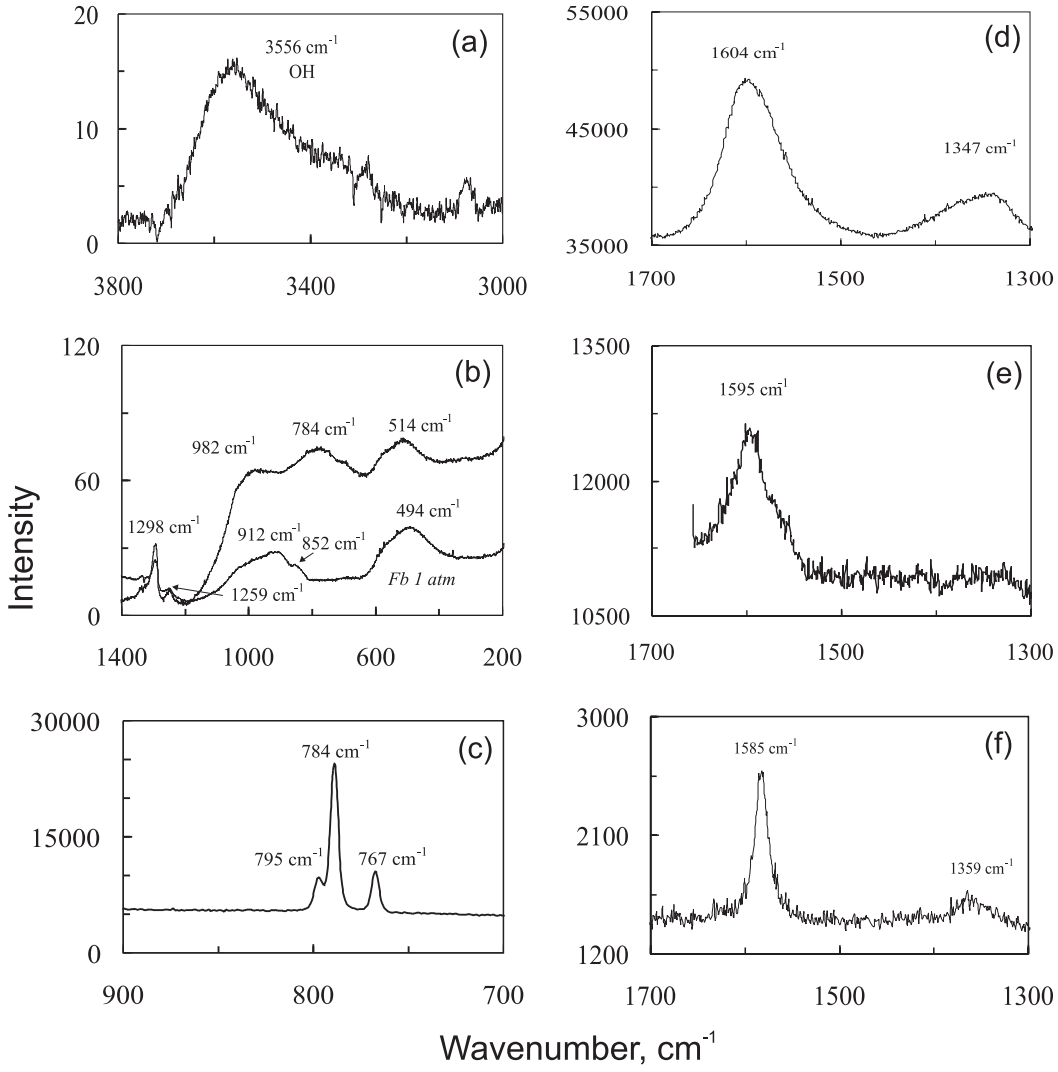

Fig. 7. Raman spectra. (a) Fb231-gl: a broad, asymmetric band at $\sim$3560 cm^{-1} is assigned to the stretching vibrations of the O–H band, either in molecular or hydroxyl groups bonded to the silicate network. (b) Comparison between the low frequency (1400–200 cm^{-1}) of the carbon- and hydrogen-bearing glasses in Fb 1 atm and Fb231-gl. The pronounced peak at 784 cm^{-1} is assigned to the Si–OH or Si–C bond. (c) Raman spectra of a synthetic Si–C crystal. (d)–(f) are Raman spectrum of graphite over the range 1700–1300 cm^{-1}. (d) Fine dispersed graphite in Fb148-gl. (e) Thin hexagonal tablets of graphite crystal in Fb231-gl. (f) Graphite disc that was located in a top of the sample during experiment (see Fig. 1b).

Following Lespade *et al.* (1982) and Rouzaud *et al.* (1983), bands at 1347–1355 cm^{-1} and at 1585–1604 cm^{-1} are attributed to the C–C stretching region of graphite with various degrees of crystal order. With increasing disordering, the 1582 cm^{-1} band broadens and moves to higher frequency, and a broad band appears at $\sim$1350 cm^{-1} and increases in intensity. According to these observations, the extremely fine dispersed black particles in the region of dendritic microstructure represent poorly crystallized graphite or amorphous carbon.

Ion probe analysis of the $^{1}H^{+}/^{30}Si^{+}$ ratio in the glasses

Polished thin sections were prepared to measure the $^{1}H^{+}/^{30}Si^{+}$ ratio in the glasses (sample Fb231-gl) with a Cameca IMS 3f ion microprobe (Institute of Microelectronics and Informatics, Russian Academy of Sciences, Yaroslavl'). Samples were ultrasonically cleaned in pure alcohol, baked at 40°C overnight, coated with gold, and kept at 40°C until introduction into the ion microprobe. The intensities on peaks $^{1}H^{+}$ and $^{30}Si^{+}$ were recorded under bombardment of an O_2^- primary beam of 10–15 nA intensity and 10 μm in size, at mass resolution of 1200 and with an energy filtering of 100 ± 20 V. H_2O contents of 1·65 ± 0·03 wt % H_2O were obtained using the calibration curves of Sobolev & Chaussidon (1996). Those workers have calibrated the $^{1}H^{+}/^{30}Si^{+}$ ratios versus the wt % H_2O/wt % SiO_2 ratios in the range 0·09–8 wt % H_2O. No strong matrix effects were found on standards ranging in SiO_2 content between 49 and

71 wt %. It is necessary to note that our experiment has been carried out at low fO_2 and the hydrogen in the glasses can exist in other forms than H_2O. Consequently, the H_2O contents should be considered as maximum values.

Step-heating extraction under oxidizing conditions

During step-heating extraction, the sample is heated under a moderate oxygen pressure. The temperature is chosen in such a way that it corresponds to the extraction of given carbon species (see Pineau & Javoy, 1994, for details). In mid-ocean ridge basalt-type glassy samples the carbon extracted above 900°C is considered to represent the carbon dissolved in the glass (mainly present in the form of carbonate ions). The entire H_2O content is extracted between 200°C and melting temperature (usually 1300–1350°C). Each carbon fraction (in the form of CO_2) and H_2 was isotopically analysed on a Finnigan Mat delta E mass spectrometer with appropriate blank corrections.

Two samples (Fb148-gl and Fb150-gl) were studied. The first one is composed of the glassy fraction still coated on one side by part of the graphite disc. The second had this graphite removed by a careful polishing. To burn the graphite present in sample Fb148-gl, the 900°C step was repeated until the amount of carbon came close to the blank value. Then, a single step at 1300°C extracted the remaining carbon. The amount of carbon and water extracted at each temperature step and the corresponding isotopic composition are given in Table 3. Several comments can be made. (1) During the two experiments, the H_2O was extracted during the 900°C step, and the amounts vary by a factor of two (1·0 ± 0·1 and 2·01 ± 0·05 wt % in Fb148-gl and Fb150-gl, respectively). The δD values of the water extracted from both samples are similar (−123 and −133‰). The preparation of sample fb150-gl (graphite elimination by polishing) may have introduced some water, not removed by the degassing step. Nevertheless, this adsorbed water should have been expressed mainly at 650°C, whereas it represents only 10% of the total water extracted. It is difficult to consider that in one case the water is inherited from the experiments and in the other it comes from an external polluting product, whereas both have the same isotopic composition. Consequently, it is considered that both measurements are correct and the variations between them are linked to heterogeneity inside the samples. (2) Sample Fb150-gl does not contain the graphite disc. The oxidation of the glass at the 650°C step is slow and corresponds in part to cleaning. Consequently, it has not been taken into consideration. On the contrary, half of the total carbon is already extracted at 900°C (in three steps) and the other half at 1300°C, which means that the reduced glass is oxidized at 900°C and that the reduced carbon content, seen by Raman exploration, is liberated in the form of CO_2 as a result of the presence of the 4 mbar oxygen pressure. The 1639 ppm C extracted from sample Fb150-gl corresponds to the sum of the 900 and 1300°C steps.

Table 3: Carbon, water, and nitrogen concentration, and $\delta^{13}C$ and δD in samples Fb148-gl and Fb150-gl by step-heating experiments

Sample number:	Fb148-gl		Fb150-gl		
Glass weight:	0·060 g		0·109 g		
Temperature:	900°C	1300°C	650°C	900°C	1350°C
Number of steps:	4	1	2	3	1
CO_2					
μmoles	1297	3·56	0·4	7·4	7·5
ppm C	1045*	46		813	826
$\delta^{13}C$	−26·4	−26·6	−28·3	−27·7	−26·9
H_2O					
μmoles	25	<blank	10	102	<blank
wt %	1·01	2·01			
δD	−123‰			−133‰	
N_2					
μmoles	0·15				
ppm N_2	270				

*Water and carbon concentrations have been calculated using the glass weight (= starting sample weight − graphite weight calculated).
The precisions on concentrations are ≤±10% for carbon, ≤±5% for water and about 20% for nitrogen. The precisions on $\delta^{13}C$ are ±0·02 for graphite (analytical precision); 0·1–0·2‰. For high-temperature steps; ±2‰ on δD.

When a graphite disc is present (Fb148-gl), a rather long oxidation at 900°C is needed (210 min). During the first three 900°C steps, the oxygen is used to burn the graphite; however, during the fourth combustion step, when most graphite has already gone, part of the oxygen may oxidize the reduced glass and part of the amorphous carbon may be extracted. Nevertheless, 1045 ppm of carbon was extracted during the 1300°C step. This represents 63% of the carbon extracted from Fb150-gl.

The H/C atomic ratios are very similar, 14·04 and 13·69 for Fb150-gl and Fb148-gl, respectively. This is consistent with the possibility that the samples are heterogeneous (otherwise, there would be no reason to preserve the H/C ratio). This means that when the water content increases the dissolved carbon content also increases. This is an important result, indicating that the behaviour of the two elements (C and H) is closely related and certainly linked to the opposite effects of

water (depolymerization) and carbon (polymerization) on the silicate network.

The carbon isotopic composition was measured (see Table 2). The $\delta^{13}C$ of the starting graphite was $-26{\cdot}5 \pm 0{\cdot}1$‰. In Fb150-gl, it is a little lighter ($-27{\cdot}3$‰), whereas it is identical for Fb148-gl ($-26{\cdot}6$‰). The relationship between these two values is explained by a loss of CO_2 (enriched in ^{13}C) during the last oxidation step at 900°C. The isotopic difference observed between the graphite of the disc and the carbon present in Fb150-gl gives a first measurement of the isotopic fractionation between these two carbon phases of 0·8‰.

DISCUSSION

Comparison with previous studies

The mean H_2O contents deduced from ion microprobe analysis (1·65 wt %) and by stepwise heating experiments (1–2 wt %) are compatible with the amount of oxygen liberated during the reduction of the ferrobasaltic melt to form the Fe metallic phase and equal to 1·96 wt % H_2O for Fb150-gl and 1·83 wt % H_2O for Fb231-gl. These values are at the lower limit of the $1{\cdot}7 \pm 0{\cdot}1$ to 4·8 wt % H_2O (Taylor & Green, 1987) in soda-melilite and jadeite glasses respectively, equilibrated with a methane-rich fluid (3 GPa, 1300°C, $\Delta \log fO_2^{IW} = -5$). Such glasses contained between 0·1 and 0·2 wt % of carbon, which is also compatible with the amount of carbon found in our reduced ferrobasalts and in alkali and tholeiitic basalts with a CH_4-dominated fluid at 1–2 GPa and 1200°C, buffered by graphite, iron and wüstite (Holloway & Jakobsson, 1986). In the later case, 3·7–4·8 wt % H_2O was found, which is two to three times higher than in our samples. This may be explained by the absence of a significant degree of reduction (the reduction of the melt being controlled by hydrogen diffusion through the Pt capsule).

Under more oxidizing conditions, the solubilities of H_2O and CO_2 are much higher than those found in the present study. For example, Pan *et al.* (1991) found that 3350 ppm C in basaltic melt equilibrated with CO_2 at 15 GPa and 1400–1600°C; Dixon *et al.* (1995) and Pineau *et al.* (1998) found up to 8·3–8·6 wt % H_2O at 0·5 GPa and 1200–1250°C in basalt and basaltic andesite. All these results suggest that C and H solubility increases when the fO_2 in the C–O–H system changes from IW or below to ~FMQ.

Mechanisms of C and H dissolution

Eggler & Baker (1982), Holloway & Jakobsson (1986), Luth *et al.* (1987) and Taylor & Green (1987) have shown that equilibration of a silicate melt with a CH_4-, H_2-bearing fluid phase causes a reduction of the silicate network to give an 'oxidized bond' such as O–H or O–C. Under fO_2 equivalent conditions, but without a CH_4- and H_2-rich phase, the behaviour of C and H seems to diverge. Our data indicate that in the presence of graphite the slow and continuous introduction of hydrogen reduces FeO and forms an 'oxidized' hydrogen component, dominantly OH^- and, to a lesser extent, H_2O. The predominance of the OH^- group over H_2O may indicate the possible presence of molecular H_2. For example, Luth *et al.* (1987) have detected the presence of molecular H_2 in hydrous glasses in the system Na_2O–Al_2O_3–SiO_2–H_2.

Rather small amounts of carbon can be dissolved in the melt in a neutral form (atomic carbon?), possibly forming amorphous C during quenching, with trace amounts of CO_2 and CO_3^{2-}. The spectroscopic data indicate the beginning of the silicate network reduction, with the formation of Si–C bonds. Such a reduction of the silicate network can become more important as the reduction process progresses and will favour the formation of a non-stoichiometric network component containing units with an O/Si ratio <2. The formation of Si–C bonds can be described by the following equation for $[Si_2O_7]^{6-}$:

$$[Si_2O_7]^{6-}\ (\text{melt}) + C\ (\text{graphite}) = \{SiC\}\ (\text{melt}) + [SiO_4]^{4-}\ (\text{melt}) + O^{2-} + O_2\ (\text{melt}) \quad (7)$$

and

$$[Si_2O_7]^{6-}\ (\text{melt}) + H_2\ (\text{melt}) = \{Si{-}O\}\ (\text{melt}) + [SiO_4]^{4-}\ (\text{melt}) + 2(OH)^-\ (\text{melt}) \quad (8)$$

where { } represents an unidentified location in the silicate network and [ ] a melt-unit or complex.

These reactions correspond to a network depolymerization by a change in the activity of network-modifying oxides (Taylor & Green, 1987), which may influence the viscosity and density of the melt.

The transport of volatile constituents in the Earth

The transport of volatile constituents from planetary interiors to their surface may provide an important part of the atmosphere and hydrosphere, the rest being provided by late additions (late veneer). It is generally agreed that, on terrestrial planets, this transport is strongly dependent on the solubility of the volatile species in magmas. Our experiments on the reduction of a ferrobasalt by an influx of hydrogen in the presence of graphite is an attempt to mimic some transition stages during the melting event produced by a great impactor which is commonly invoked in Earth formation models (e.g. Javoy, 1998, 1999). The magmas formed during this event would have had a composition varying from ferroan komatiites to reduced ferrobasalt. The H_2 present in the primitive Earth body (corresponding to

~400–500 ppm 'virtual' H_2O if oxidized) would have reduced the FeO to produce OH groups dissolved in the melt whereas graphite would remain stable under these conditions. This is a simple way to explain the formation of the atmosphere–hydrosphere system outgassed from the reduced primitive Earth. When the late, more oxidized, volatile additions (late veneer) started to be recycled, the magmas would become more and more oxidized and dissolve more water and carbon (in the form of carbonate ions).

CONCLUSIONS

It has been demonstrated that the interaction between a graphite–hydrogen system and Fe-bearing melt (ferrobasalt) at 3·7 GPa, 1520–1600°C and $fO_2 = IW - 2{\cdot}5$ generates a general reduction of the silicate melt and C and H dissolution by the formation of C–O–H volatile species.

Under our experimental conditions, hydrogen appears much more reactive than carbon, and forms dissolved OH^-, H_2O, and H_2. Carbon is mainly dissolved in the melt as amorphous or atomic C. The excess of C is expressed as well-crystallized graphite in equilibrium with the melt. It is possible that transitional oxidized forms of C exist. An isotopic fractionation of 0·8‰ was measured between graphite and dissolved or amorphous carbon for a temperature of 1560 ± 40°C.

The existence of silicon–carbon bonds is proposed, with the possible consequence of a depolymerization of the silicate network and changes in the activity of network-modifying oxides.

The amounts of C–O–H volatile dissolved in melts at low fO_2 and 3·7 GPa (corresponding to ~100 km depth in the mantle) are particularly low. Carbon solubility is about an order of magnitude less than that of H_2O (about 2 wt % H_2O and 0·2 wt % C).

These conclusions confirm the earlier works of Holloway & Jakobsson (1986) and Taylor & Green (1987), showing the dissolution of CH_4 in reduced silicate melts to be associated with H_2O and OH formation (from $\log fO_2 = IW$ to $\log fO_2 = IW - 5$ log units). Similar to the work of Taylor & Green (1987), which was carried out at lower fO_2 ($fO_2 = IW - 5$ log units) and 3 GPa (on jadeite and soda-melilite compositions), we did not detect the presence of dissolved carbonate ion in the experimental melts. The formation of CO_3^{2-} and CO_2 in basic magmas at fO_2 values values below the IW oxygen buffer seems to require higher fO_2 values than that of H_2O and OH species or a depletion of hydrogen in the starting material.

In conclusion, it appears that the chemical evolution of carbon and hydrogen during the very reduced episode of early mantle evolution could be very much influenced by the presence of iron-rich melts. The iron reduction in these melts is a way of providing the transformation of the reduced forms of hydrogen and carbon that were present in the early mantle (e.g. Javoy 1995, 1997, 1999) into the now dominant mantle forms (hydroxyl group, molecular water and carbonate ion).

ACKNOWLEDGEMENTS

This work was made possible through a PAST position provided to A. Kadik by the MENRST. Additional support was provided through the Russian Foundation of Fundamental Investigation, Grant 99-05-65479. We are grateful to Dr D. R. Neuville for Raman spectroscopy of our samples at the Université de Paris and fruitful discussion. Dr V. Plotnichenko and Dr V. Koltashev kindly analysed selected glasses by Raman spectroscopy at the General Physics Institute of RAS (Moscow). Hubert Remy is thanked for his help during electron mocroprobe analysis, and Michel Girard and Jean Jacques Bourrand for their technical assistance. Professor R. T. Arculus and an anonymous reviewer are thanked for their constructive comments. This paper is IPGP contribution 1940 and CNRS contribution 352.

REFERENCES

Arculus, R. J. (1985). Oxidation status of the mantle: past and present. *Annual Review of Earth and Planetary Sciences* **13**, 75–95.

Arculus, R. J., Holmes, R. D., Powell, R. & Richter, K. (1990). Metal–silicate equilibria and core formation. In: Newsom, H. E. & Jones, J. H. (eds) *Origin of the Earth*. Houston, TX: Lunar and Planetary Institute; New York: Oxford University Press, pp. 251–271.

Ariskin, A. A., Borisov, A. A. & Barmina, G. S. (1993) Simulating iron–silicate melt equilibrium in basaltic systems. *Geochemistry International* **30**, 13–22.

Ballhaus, C. (1993). Redox states of lithospheric and asthenospheric upper mantle. *Contributions to Mineralogy and Petrology* **114**, 331–348.

Ballhaus, C. (1995). Is upper mantle metal-saturated? *Earth and Planetary Science Letters* **132**, 75–86.

Bohlen, S. R. & Boettcher, A. L. (1982). The quartz–coesite transformation: a precise determination and the effects of other components. *Journal of Geophysical Research* **87**, 7073.

Chou, I.-M. (1987). The oxygen buffer and hydrogen sensor techniques at elevated pressures and temperatures. In: Ulmer, G. C. & Barens, H. L. (eds) *Hydrothermal Experimental Techniques*. John Wiley, New York, pp. 61–99.

Daniels, L. R. M. & Gurney, J. J. (1991). Oxygen fugacity constraints on the southern African lithosphere. *Contributions to Mineralogy and Petrology* **108**, 154–161.

Debernardi, A., Ulrich, C., Syassen, K. & Cardona, M. (1999). Raman linewidths of optical phonons in 3C–SiC under pressure: first-principles calculations and experimental results. *Physical Review B* **59**(10), 6774–6783.

Dianov, E. M., Bubnov, M. M., Gurianov, A. N., Hopin, V. F., Kryukova, E. B., Plotnichenko, V. G., Rybaltovskii, A. A. & Sokolov, V. O. (2000). Phosphosilicate glass optical fibres—a promising material for Raman lasers. *Proceedings of ECOC 2000, 3–7 September, Munich, 3*, pp. 135–136.

Dixon, J. E., Stolper, E. M. & Holloway, J. R. (1995). An experimental study of water and carbon dioxide solubilities in mid-ocean ridge basaltic liquids. I. Calibration and solubility models. *Journal of Petrology* **36**, 1607–1631.

Eggler, D. H. & Baker, D. (1982). Reduced volatiles in the system C–O–H: implications to mantle melting, fluid formation, and diamond genesis. In: Akimoto, S. & Manghnani, M. (eds) *High Pressure Research in Geophysics*. Tokyo: Center for Academic Publications, pp. 237–250.

Fine, G. & Stolper, E. (1985). The speciation of carbon dioxide in sodium aluminosilicate glasses. *Contributions to Mineralogy and Petrology* **91**, 105–121.

Galimov, E. M. (1998). Growth of the Earth's core as a source of its internal energy and a factor of mantle redox evolution. *Geochemistry International* **36**, 673–675.

Hillgren, V. J., Drake, M. J. & Rubie, D. C. (1994). High pressure and temperature experiments on core–mantle segregation in the accreting Earth. *Science* **264**, 1442–1445.

Holloway, J. R. (1981). Volatile interactions in magmas. In: Newton, R. S., Navrotsky, A. & Wood, B.J. (eds) *Thermodynamics of Minerals Nad Melts*. Advances in Physical Geochemistry, 273–293.

Holloway, J. R. & Jakobsson, S. (1986). Volatile solubilities in magmas: transport of volatiles from mantles to planet surface. *Journal of Geophysical Research* **91**(B4), D505–D508.

Holloway, J. R., Pan, V. & Gudmundsson, G. (1992). High-pressure fluid-absent melting experiments in the presence of graphite: oxygen fugacity, ferric/ferrous ratio and dissolved CO_2. *European Journal of Mineralogy* **4**, 105–114.

Javoy, M. (1995). The integral Enstatite Chondrite model of the Earth. *Geophysical Research Letters* **22**, 2219–2222.

Javoy, M. (1997). The major volatile elements of the Earth: origin, behavior, and fate. *Geophysical Research Letters* **24**, 177–180.

Javoy, M. (1998). The birth of the Earth's atmosphere: the behaviour and fate of the major elements. *Chemical Geology* **147**, 11–25.

Javoy, M. (1999). Chemical Earth model. *Comptes Rendus de l'Académie des Sciences, Sciences de la Terre et des Planètes* **329**, 537–555.

Kadik, A. A. (1996). Formation of carbon species in terrestrial magmas. In: Farley, K. A. (ed.) *Volatiles in the Earth and Solar System. American Institute of Physics Conference Proceedings* **341**, 106–114.

Kadik, A. A. (1997). Evolution of Earth's redox state during upwelling of carbon-bearing mantle. *Physics of the Earth and Planetary Interiors* **100**, 157–166.

Lespade, P., Al-Jishi, R. & Dresselhaus, M. S. (1982). Model for Raman scattering from incompletely graphitized carbons. *Carbon* **5**, 427–431.

Litvin, Yu. A. (1989). On the technique of high-pressure studying phase equilibrium of ferro-ferrous magmatic melts. *Geochimia* (8), 1234–1242 (in Russian).

Long, D. A. (1977). *Raman Spectroscopy*. New York: McGraw–Hill, 276 pp.

Luth, R. W., Mysen, B. O. & Virgo, D. (1987). Raman spectroscopic study of the solubility behavior of H_2 in the system Na_2O–Al_2O_3–SiO_2–H_2. *American Mineralogist* **72**, 481–486.

Mattioli, G. S., Baker, B., Rutter, M. G. & Stolper, E. M. (1989). Upper mantle oxygen fugacity and relationship to metasomatism. *Journal of Geology* **97**, 521–536.

Mysen, B. O. (1998). Interaction between aqueous fluid and silicate melt in the pressure and temperature regime of the Earth's crust and upper mantle. *Neues Jahrbuch für Mineralogie, Abhandlungen* **172**(2–3), 227–244.

Mysen, B. O. & Virgo, D. (1986) Volatiles in silicate melts at high pressure and temperature, 2. Water in melts along the join $NaAlO_2$–SiO_2 and a comparison of solubility mechanisms of water and fluorine. *Chemical Geology* **57**, 333–358.

Neuville, D. R. & Mysen, B. O. (1996). Role of aluminium in the silicate network: *in situ*, high-temperature study of glasses and melts on the joint SiO_2–$NaAlO_2$. *Geochimica et Cosmochimica Acta* **60**, 1727–1737.

Newman, S., Stolper, E. M. & Epstein, S. (1986). Measurement of water in rhyolitic glasses: calibration of an infrared spectroscopic technique. *American Mineralogist* **71**, 1527–1541.

O'Neill, H. St. C. (1991). The origin of the Moon and the early history of the Earth—a chemical model. Part 2: The Earth. *Geochimica et Cosmochimica Acta* **55**, 1159–1172.

O'Neill, H. St. C. & Pownceby, M. I. (1993). Thermodynamic data from redox reactions at high temperatures. I. An experimental and theoretical assessment of the electrochemical method using stabilized zirconia electrolytes, with revised values for the Fe–'FeO', Co–CoO, Ni–NiO and Cu–Cu_2O oxygen buffers, and new data for the W–WO_2 buffer. *Contributions to Mineralogy and Petrology* **114**, 296–314.

O'Neill, H. St. C. & Wall, V. J. (1987). The olivine–orthopyroxene–spinel oxygen geobarometer, the nickel precipitation curve and the oxygen fugacity of the Earth's upper mantle. *Journal of Petrology* **28**, 1169–1191.

Pan, V., Holloway, J. R. & Hervig, R. L. (1991). The pressure and temperature dependence of carbon dioxide solubility in tholeiitic basalt melts. *Geochimica et Cosmochimica Acta* **55**, 1587–1595.

Parkinson, I. J. & Arculus, R. J. (1999). The redox state of subduction zones: insights from arc-peridotites. *Chemical Geology* **166**, 409–423.

Pineau, F. & Javoy, M. (1994). Strong degassing at ridge crests: the behavior of dissolved carbon and water in basalt glasses at 14°N, Mid-Atlantic Ridge. *Earth and Planetary Science Letters* **123**, 179–198.

Pineau, F., Shilobreeva, S., Kadik, A. & Javoy, M. (1998). Water solubility and D/H fractionation in the system basaltic andesite–H_2O at 1250°C and between 0·5 and 3 kbars. *Chemical Geology* **147**, 173–184.

Pouchert, C. G. (1981). *The Aldrich Library of Infrared Spectra*, 3rd edn. Milwaukee, WI: Aldrich Chemical Co., 1203 pp.

Rouzaud, J. N., Oberelin, A. & Beny-Baddez, C. (1983). Carbon films structure and microtexture (optical and electron microscopy, Raman spectroscopy). *Thin Solid Films* **105**, 75–96.

Sobolev, A. V. & Chaussidon, M. (1996). H_2O concentrations in primary melts from supra-subduction zones and mid-oceanic ridges: implications for H_2O storage and recycling in the mantle. *Earth and Planetary Science Letters* **137**, 45–55.

Stolper, E. (1982). The speciation of water in silicate melts. *Geochimica et Cosmochimica Acta* **46**, 2609–2620.

Swisher, J. H. (1968). Thermodynamics of carbides formation and graphite solubility in the CaO–SiO_2–Al_2O_3 system. *Transactions of the Metallurgical Society of AIME* **242**, 2033–2037.

Taylor, W. R. & Foley, S. F. (1989). Improved oxygen-buffering techniques for C–O–H fluid-saturated experiments at high pressure. *Geophysical Research Letters* **94**(B4), 4146–4158.

Taylor, W. R. & Green, D. H. (1987). The petrogenetic role of methane: effect on liquidus phase relations and the solubility mechanism of reduced C–H volatiles. In: Mysen, B. O. (ed.) *Magmatic Processes: Physicochemical Principles. Geochemical Society, Special Publications* **1**, 121–138.

Ulmer, P. & Luth, R. W. (1991). The graphite–COH fluid equilibrium in P, T, fO_2 space. An experimental determination to 30 kbar and 1600°C. *Contributions to Mineralogy and Petrology* **106**, 265.

Wanke, H. (1981). Constitution of terrestrial planets. *Philosophical Transactions of the Royal Society of London, Series A* **303**, 287–302.

Wood, B. J. (1995). Storage and recycling of H_2O and CO_2 in the Earth. In: Farley, K. A. (ed.) *Volatiles in the Earth and Planetary Solar System. American Institute of Physics Conference Proceedings* **341**, 3–21.

Wood, B. J., Bryndzia, L. T. & Johnson, K. E. (1990). Mantle oxidation state and its relationship to tectonic environment and fluid speciation. *Science* **248**, 337–345.